Journal of Solid State Chemistry 184 (2011) 1523–1529

Contents lists available at ScienceDirect

Journal of Solid State Chemistry

journal homepage: www.elsevier.com/locate/jssc

Infrared absorptive properties of Al-doped ZnO divided powder

H. Serier, A. Demourgues, J. Majimel, M. Gaudon *

CNRS, Université de Bordeaux, ICMCB, 87 avenue du Dr. A. Schweitzer, Pessac F-33608, France

ARTICLE INFO

Article history:
Received 25 October 2010
Received in revised form
23 March 2011
Accepted 29 March 2011
Available online 15 April 2011

Keywords:
ZnO
Optical properties
Infrared

ABSTRACT

Al-doped ZnO powders were synthesised by a Pechini process in order to obtain visible non-absorbent and near-Infrared absorbent particles. Firstly, it has been shown that synthesis under argon combined with the lowest synthesis temperatures (700 °C) allows getting the optimal properties for pure ZnO compounds due to creation of n-type defects segregated on oxide grain surface (Zn/O ratio superior to 1). Nevertheless, the near-Infrared absorption properties of the pure ZnO compounds remain low. The Al^{3+} doping of ZnO compounds was then investigated. The Al solubility limit inside ZnO doped compounds decreases drastically with the grain size, i.e. with the synthesis temperature. Then, the Al cations distribution varies inside ZnO grains, Al^{3+} segregation at the grain surfaces taking place for high synthesis temperatures. The optimal optical properties (high near-Infrared absorption) are reached combining Al-doping and adequate synthesis conditions: annealing under argon at low temperatures. In these conditions, the highest extrinsic (via Al doping) and intrinsic n-types defects rates are indeed reached.

1. Introduction

Al-doped ZnO oxide is one of the most used transparent conductive oxides (TCOs). TCOs are used as transparent electrodes (opto-electronic devices), or as thermal insulator films in smart windows (low emissive windows) [1–9]. Al^{3+} substitution for Zn^{2+} cations remains nevertheless difficult because they differ on their oxidation state, their ionic radius and their coordination number preference. Numerous publications have dealt with providing a more accurate estimation of the Al^{3+} solubility limit in ZnO [10–20]. It can be reminded that TCOs conductivity is directly linked to the free-carriers' concentration. The free-carriers are correlated to the intrinsic ZnO n-type defects in addition to the extrinsic n-type defects due to Al^{3+} inserted cations. Furthermore, TCOs as doped ZnO possess transmission/infrared absorption phenomena that are linked to one characteristic parameter: the plasma frequency ω_p, comparable to a "cut-off frequency" with regard to the electronic transport properties and therefore the refractive index of the material [21]. The plasma frequency is directly related to the free carrier concentration. The sharp variation of the optical indexes around plasma frequency induces visible transparency and Infrared absorption. An abrupt decrease of the n index and abrupt increase of the k absorption coefficient, which are related to the Kramers–Kronig relation [22,23], can then be observed. The direct measurement of the diffuse reflection of a powder sample collected with an integrating sphere leads to a qualitative assessment of TCOs properties. Thus, a decrease of the sample diffuse reflection due to the increase of the k coefficient should be observed [24–26].

Various synthesis temperatures under argon atmosphere leading to different optical characteristics on pure ZnO and doped ZnO were investigated and compared. The synthesis process used is a Pechini process, allowing the obtaining of a crystalline material with low annealing temperature (typically 700 °C). The impact of the synthesis atmosphere and temperature on the n-type native defects concentration is discussed on the basis of the Al^{3+} cations concentration and homogeneity and the materials' optical properties.

In a first part, pure ZnO compounds synthesised under argon ($pO_2 \approx 10^{-5}$ atm) and air combined with low or high synthesis temperatures were compared in order to evidence the crucial role of the synthesis atmosphere on the sample optical properties.

In a second part, on the basis of Al-doped ZnO powder synthesis prepared under argon atmosphere, the Al solubility limit versus synthesis temperature (700 °C, 850 °C) is characterised and linked to the Al distribution inside the zincite crystallites combining X-ray diffraction and transmission electronic microscopy. These results are correlated to the optical absorption properties of the various synthesised samples.

2. Experimental

The doped ZnO oxides were prepared by a Pechini process, which allows the synthesis of sub-micronic powder at low temperature [27,28]. Briefly, this synthesis process is based on

* Corresponding author.
E-mail address: gaudon@icmcb-bordeaux.cnrs.fr (M. Gaudon).

0022-4596/$ - see front matter © 2011 Elsevier Inc. All rights reserved.
doi:10.1016/j.jssc.2011.03.041

the chelating of metal ions by a hydroxyl acid such as citric acid in order to form stable homogeneous solutions. The addition of a polyalcohol such as ethylene glycol enables a poly-esterification of the organic reagents and the formation of a viscous brown resin by heating on a hotplate. The synthesis was performed with metal nitrates (M), citric acid (CA) and ethylene glycol (EG) as starting materials obeying to the molar ratio 1:4:4. A first annealing under air at low temperature (400 °C for 5 h) was proceeded in order to remove the organic precursors; the obtained black powder was then ground in an agate mortar and heated to 700–1200 °C for 10 h under air or argon atmosphere.

UV–vis–NIR absorption properties were investigated by diffuse reflectance spectroscopy using a Cary 5000E spectrophotometer equipped with an integrating sphere in the wavelength region between 200 and 2500 nm. Samples were placed in a Suprasil® cell equipped with a quartz window; halon standard (6 mm deep and 1 g/cm^3 density) was used as a white reference.

The sizes of the sub-micronic grains and agglomerates were roughly evaluated by scanning electronic microscopy (SEM). SEM micrographs was recorded with a HITACHI 4500-I apparatus fit out with a field emission gun (SEM-FEG) working at 3.0 kV. Such equipment allows a high spatial resolution (roughly equal to 5 nm) while operating at such low accelerating voltages. Transmission electronic microscopy (TEM) was performed on TECNAI F20 equipment with a field emissive gun, operating at 200 kV and with a point resolution of 0.24 nm. TEM samples were prepared from the dispersion of few milligrams of powder in ethanol; a homogeneous suspension was obtained, thanks to powder particles desegregation in ultrasonic bath. One drop of the solution was finally deposited on a Formvar/Carbon copper grid. Chemical cartographies were obtained using an EDX detector.

The zeta-potential measurements were done on a Zetasizer 3000HD, Malvern Instrument. The method applied is a capillary electrophoresis associated with a Doppler effect laser. The solid particles are dispersed in aqueous solution of calibrated pH. The dispersion is then injected in a capillary cell in which an electric field is pulsed to accelerate in opposite directions positively and negatively charged particles. The speed of the particles is measured from their Doppler effect versus the applied field for each solution pH. The zeta-potential of the particles versus the solution pH was then obtained.

X-ray diffraction patterns were collected using a PANalytical X'Pert MPD PW 3040 with Cu$K\alpha$1 radiation ($\lambda = 1.540562$ Å) and the measurements were performed with a scan step of 0.02° in the 2θ range from 5° to 130°. The Fullproof programme was used for full pattern matching and structural refinements by Rietveld method [29,30]. Fourier transforms and Fourier differences between experimental and calculated data were also proposed, thanks to Fullproof software.

3. Results and discussion

3.1. Investigations on pure ZnO compounds

The optical UV–vis–NIR diffuse reflectance of ZnO powders obtained under air or argon at different temperatures are compared (Fig. 1). For the compounds prepared under air, no near-Infrared absorption but only UV absorption relative to the ZnO band gap at about 400 nm occurs. On the opposite, for the compounds annealed under argon, the creation of n-type intrinsic defects leads to a significant near-Infrared absorption. Furthermore, the highest defects concentration (higher Infrared absorption) is reached for a low synthesis temperature. The synthesis temperature increase is always associated to a "reductive effect" (Ellingham) on oxide compounds whatever be the oxygen partial pressure used. However,

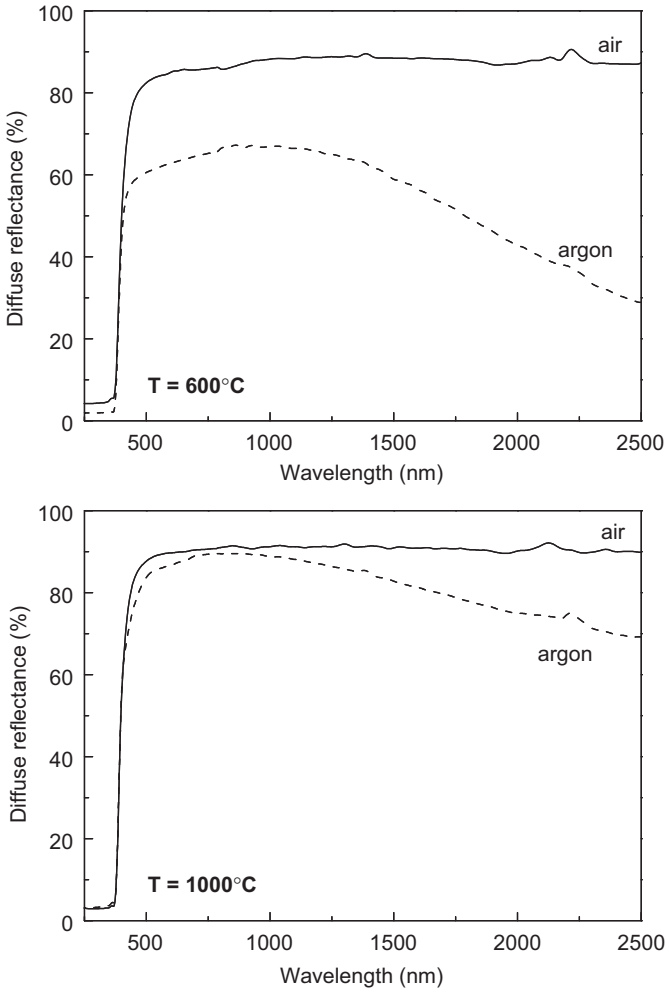

Fig. 1. Diffuse reflectance spectra of ZnO compounds obtained after thermal treatment at 600 or 1000 °C under argon or air atmospheres.

the largest surface areas (obtained for the lowest temperature synthesis) apparently lead to the highest near-Infrared absorption. The native n-types defects are certainly concentrated (segregated) on grain surfaces.

The oxides obtained after annealing at 700 °C under argon and air were analysed by X-ray diffraction. For both thermal treatments, pure oxides are obtained with roughly similar cell parameters and atomic positions: $a = 3.2487(5)$ Å, $c = 5.204(1)$ Å and $a = 3.2498(5)$ Å, $c = 5.205(1)$ Å for the compounds prepared under argon and air, respectively. In order to investigate more accurately the slight crystallographic differences caused by the variation of synthesis atmosphere, Fourier transformations were performed. The electronic maps and the electronic residues maps for various z/c plans of the two studied compounds obtained after Fourier transformation are presented in Fig. 2. The interstitial positions of zinc (n-type defect corresponding to the 2*b* empty *wyck* off positions with (1/3, 2/3, 3/4) coordinates) have been investigated in detail. The electronic residues on these interstitial positions are a bit higher for the oxide obtained under argon than for the one obtained under air (0.22 and 0.14 e Å^{-2}, respectively). Nevertheless, the small amplitude of the electronic residue density and the small difference of these electronic residues between the two synthesis routes do not allow definitively concluding on a direct correlation between the pO_2 partial oxygen pressure of the thermal treatment and the creation of Zn_i interstitial n-type defects. Hence, the atmosphere synthesis behaviour governs the optical absorption properties but these

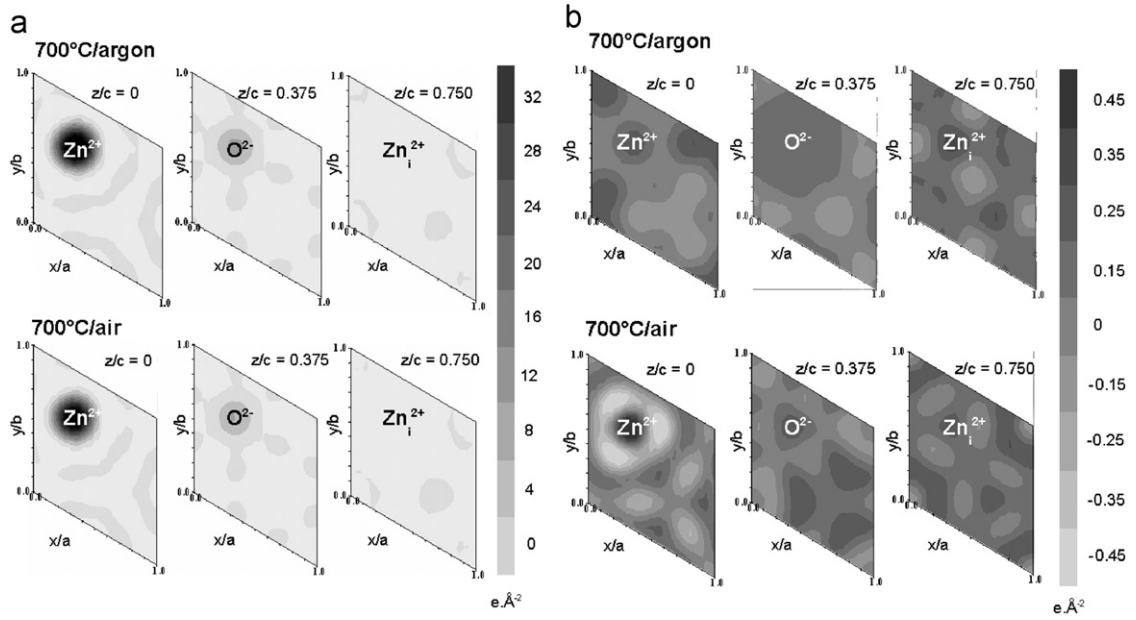

Fig. 2. Fourier transforms (a) and Fourier differences (b) maps obtained for various z/c plans of the ZnO compounds obtained at 700 °C under argon or air atmospheres.

optical properties do not seem to depend on the structural features of the oxide grain bulks.

The compounds surface (for various synthesis routes) was specifically investigated by zeta-potential measurements (Fig. 3). After annealing at 700 °C, the surfaces of the compounds obtained under air or argon are very different (Fig. 3, top part). However, for the ZnO compounds calcined under argon, the surface behaviour seems to remain the same whatever be the synthesis temperature (Fig. 3, bottom part). The zero point charge (ZPC) is known to be about 9–10 for ZnO [31–33], and to depend on the surface defects and so on the synthesis history. The ZPC of as-synthesised compounds varies between 8 and 10 depending on the synthesis temperature/atmosphere. The difference between the two samples series can be attributed to the surface reductive effect of the argon atmosphere. After the annealing under air, the sample surface could exhibit p-type defects, explaining thus the absence of Infrared absorption linked to n-type free-carriers. On the contrary, n-type surface defects should be obtained from the annealing under argon. For these latter defects, the surface behaviour seems non-dependent from the thermal treatment temperature and the n-type defect concentration per surface unit can be considered as constant. Hence, the large Infrared absorption obtained for the highly divided powder is correlated to the increase of the surface atoms concentration as the sample grain size decreases.

3.2. Investigations on Al-doped ZnO compounds

It was established that low temperatures and argon atmosphere are key features to obtain n-type ZnO oxide with high free-carriers concentration. This observation explains why a significant Infrared absorption is never obtained for Al-doped ZnO compounds prepared under air [22]. Thus, we focused on Al-doped ZnO compounds prepared under argon. Two synthesis temperatures were tested (700 and 850 °C) and their effect on the aluminium solubility in ZnO was investigated. This study was conducted comparing the diffraction patterns obtained for various Al-doped ZnO target compositions. Over the Al solubility limit, extra-peaks are detected on powder XRD patterns (Fig. 4). The impurity was characterised as spinel compound with $ZnAl_2O_4$ composition. A comparison between the two

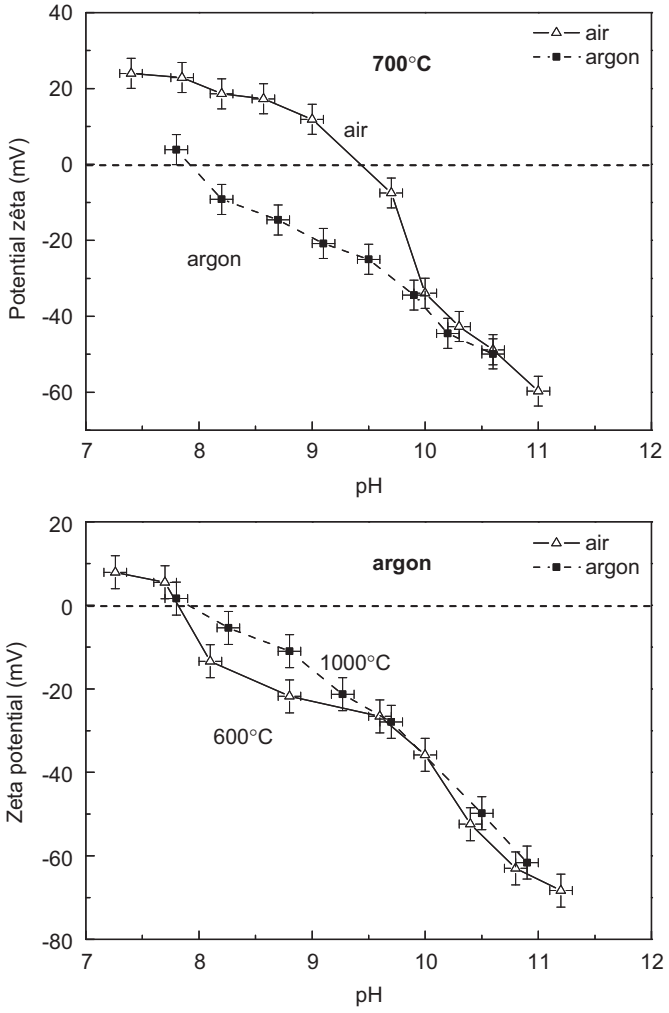

Fig. 3. Zeta-potential measurements on ZnO compound surfaces obtained after thermal treatment at 700 °C under argon or air atmospheres (top figure) or at various temperatures under argon (bottom figure).

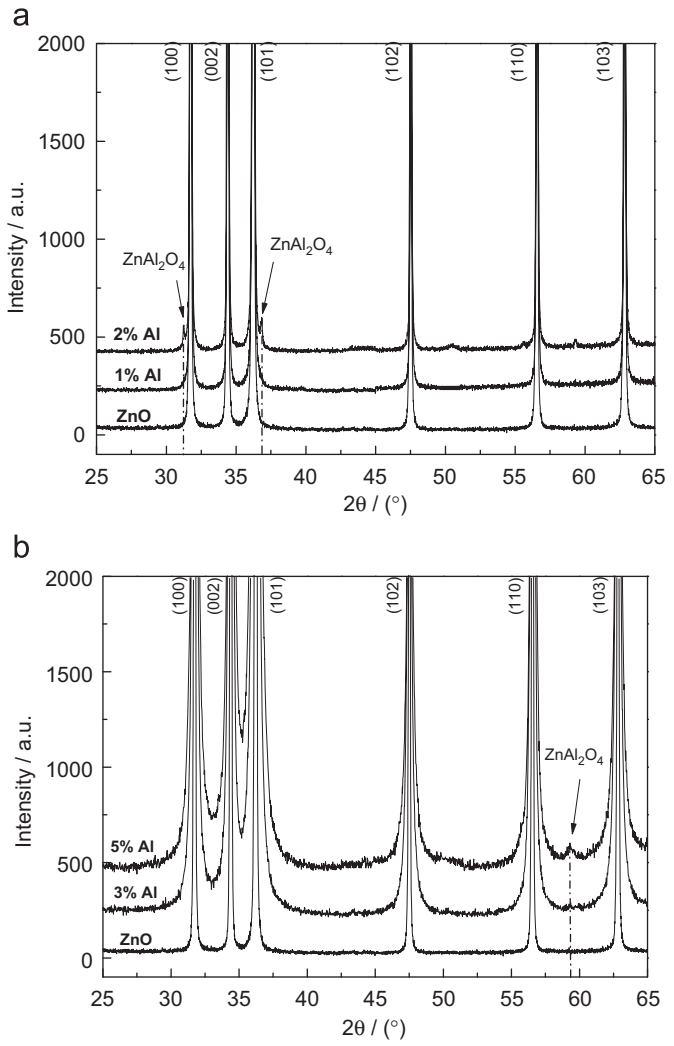

Fig. 4. X-ray diffraction patterns of various $Zn_{1-x}Al_xO$ compounds obtained after thermal treatment under argon at 850 °C (top figure) and 700 °C (bottom figure).

Table 1
Cell parameters and oxygen atomic coordinate (z(O)) of Al-doped ZnO compounds obtained after thermal treatment under argon at 850 and 700 °C.

	0%	1% Al	2% Al	3% Al	5% Al
850 °C/Ar					
a (Å)	3.24987(2)	3.24999(2)	3.25017(3)	3.25006(2)	3.24980(2)
c (Å)	5.20546(4)	5.20517(5)	5.20551(6)	5.20520(6)	5.20438(4)
z(O)	0.3805(6)	0.3826(8)	0.3819(8)	0.383(1)	0.3819(8)
700 °C/Ar					
a (Å)	3.2486(5)	3.2504(3)	3.2501(4)	3.2492(6)	3.2486(6)
c (Å)	5.2041(9)	5.2068(6)	5.2068(8)	5.205(1)	5.204(1)
z(O)	0.3820(7)	0.382(1)	0.382(1)	0.381(1)	0.381(1)

series of compound shows the aluminium solubility limit strongly depends on the thermal treatment temperature. The full width at the half maximum of the diffraction peaks is largely smaller for the 850 °C-sample than for the 700 °C-one, showing a significant crystallite growth between these two temperatures. The $ZnAl_2O_4$ phase was detected for the 850 °C-sample with the aluminium target concentration of 1 mol%, whereas $ZnAl_2O_4$ only appeared for aluminium concentration over 3 mol% for the 700 °C-sample. It is well known that large surface areas contribute to stabilise metastable phases with higher Al^{3+} rate and consequently, limit the formation of $ZnAl_2O_4$. Nevertheless, the solubility limit dependence versus temperature is here very important. Furthermore, the significant difference of the aluminium concentration introduced into these two ZnO samples has only a negligible impact on the cell parameters and the average z atomic position of the oxygen atom (Table 1). In order to illustrate the non-expected stability of the cell parameters versus the target aluminium concentration, the experimental parameters were compared to the theoretical ones calculated from the Vegard law considering that Al^{3+} substituted for Zn^{2+} ions occupy tetrahedral sites. For the calculation of the theoretical cell parameters, the Shannon radius of the Al^{3+} cation in four-fold coordination ($rAl^{3+}_{IV} = 0.39$ Å) was used (Fig. 5). The cell

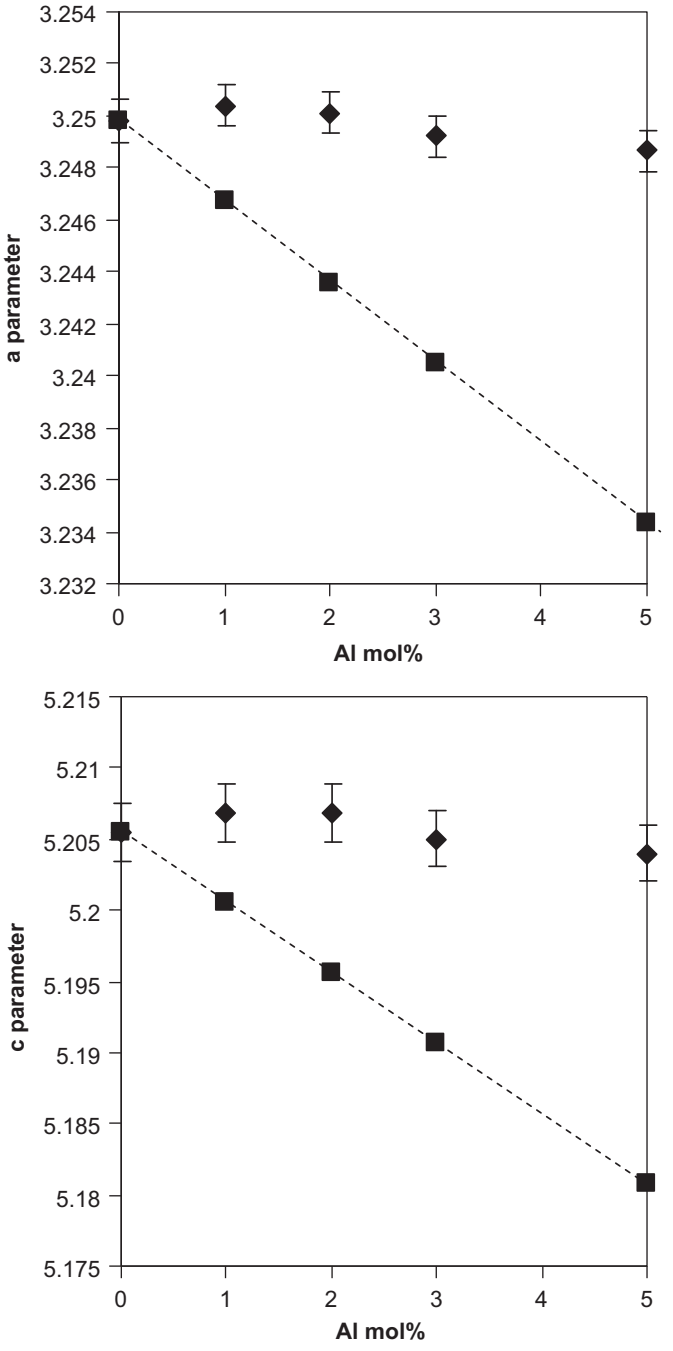

Fig. 5. Evolution of a and c cell parameters of the Al-doped ZnO compounds obtained after thermal treatment under argon at 700 °C and comparison with theoretical law calculated considering that Al^{3+} ions are substituted for Zn^{2+} ones inside the zincite structure.

parameters stability versus the aluminium concentration tends to show that the solubility limits, extracted from the detection of the spinel phase impurity, are over-estimated.

ICP titrations were performed on the Al-doped ZnO obtained under argon at 700 and 850 °C. The titration is allowed, thanks to the total solubility in slight acidic conditions of zincite phase whereas the $ZnAl_2O_4$ spinel phase is not soluble. The filtrates obtained after the selective dissolution lead thus to the real aluminium concentration incorporated into the zincite structure. The evolution of the detected concentration versus the target one is reported for both thermal treatments (Fig. 6). For aluminium concentrations lower than the solubility limit, the measured Al^{3+} concentration roughly corresponds to the introduced one (dots are placed on the 1:1 curve). For higher concentrations, the aluminium concentration detected in the filtrates remains then roughly constant. The solubility limits are about 0.4 mol% for the 850 °C-sample and about 3.5 mol% for the 700 °C-one.

At this stage, the following observations can be made: X-ray phase identification and ICP titrations led to an estimation of the aluminium solubility limit in ZnO around 3.5 mol% for the 700 °C-sample, whereas the cell parameters of the zincite are clearly not affected by the aluminium introduction. Only a segregation of the aluminium ions at the ZnO grain surface can explain the low impact of the aluminium content on the cell parameters calculated from X-ray diffraction data. This segregation can also explain the large variation of the average grain size versus the doping concentration observed by scanning electronic microscopy for various $Zn_{1-x}Al_xO$ samples annealed at a same temperature (Fig. 7). Surface segregations inducing a large surface composition perturbation; it can indeed strongly modify the crystallite growth during the annealing process. The Al^{3+} segregation was directly investigated by TEM coupled with EDX analyses, allowing the representation of samples' chemical cartographies (Fig. 8). The 3 mol% Al-doped ZnO composition prepared at 700 °C under argon exhibits a bimodal grain size distribution. The coarser grains are slightly agglomerated or are well dispersed on the sample grid (zone B on the TEM picture), whereas the finer ones formed larger and denser agglomerates (zone A on the TEM picture). The chemical compositions of both zones were quantified from EDX analyses; the aluminium concentration of the zone A is near one order of magnitude higher than the one of the zone B: the concentration of aluminium being nearly 3–5 mol% for the zone A against only 0.5–1% for the zone B. The

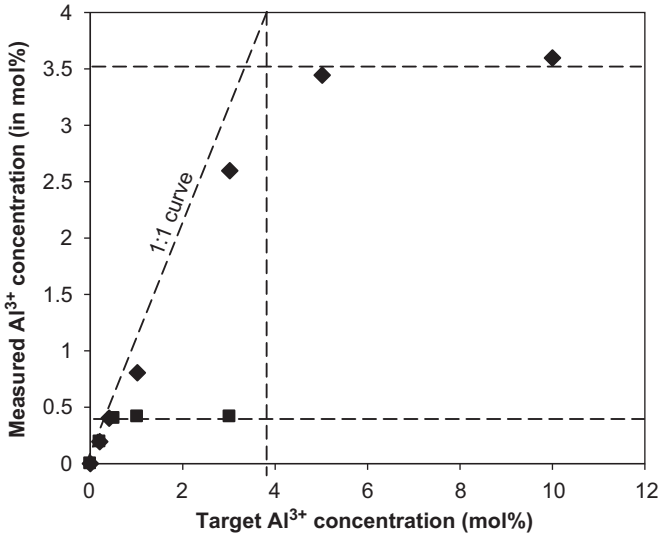

Fig. 6. ICP titration of the aluminium concentration corresponding to the one introduced in zincite structure versus the aluminium content introduced inside the Pechini sol. The results obtained after selective dissolution of the compounds synthesised at 700 and 850 °C under argon are compared: square points and rhombus points are for the 850 and 700 °C-annealed compounds, respectively.

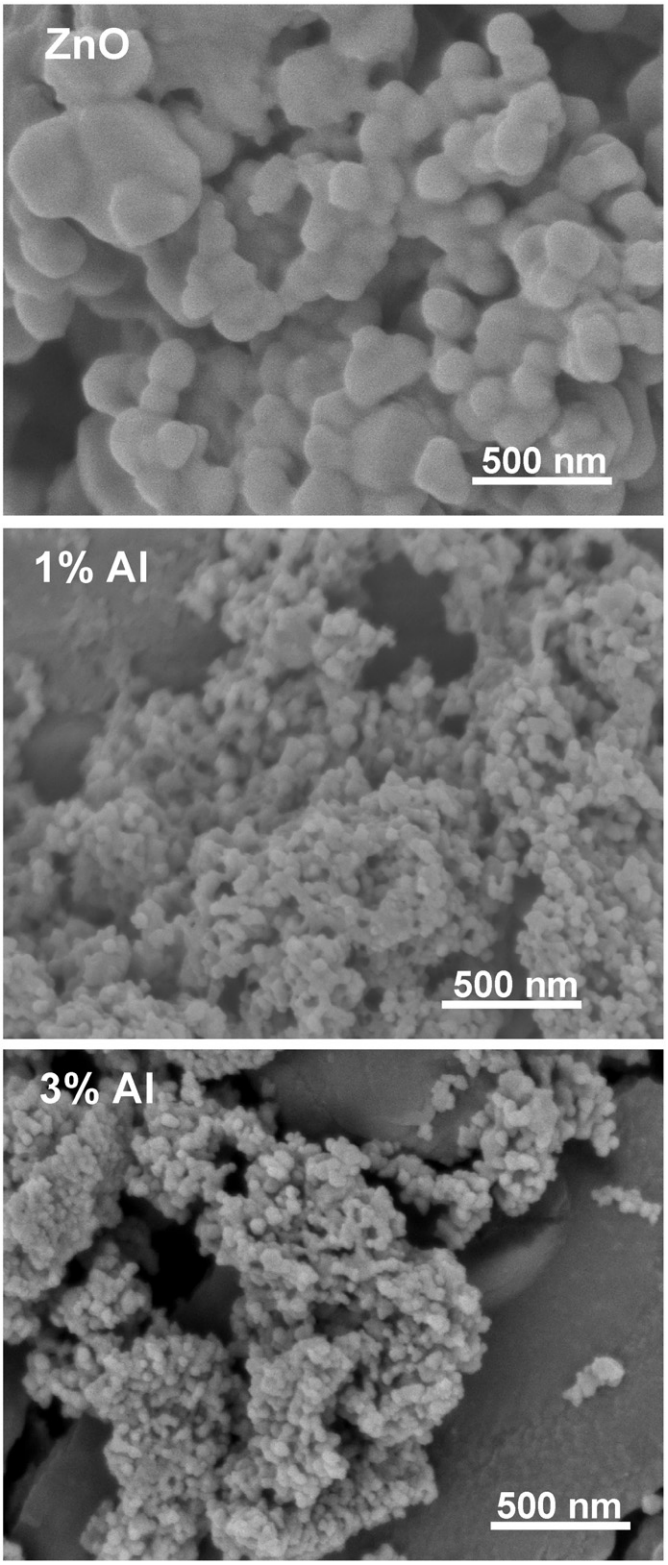

Fig. 7. SEM micrographies on pure ZnO, and 1 and 3 mol% Al-doped ZnO compounds synthesised under the same conditions (700 °C/argon).

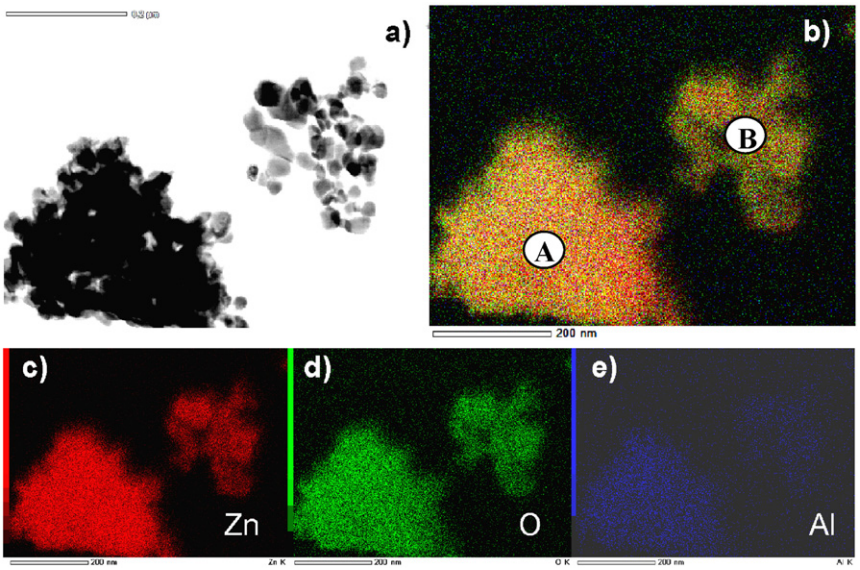

Fig. 8. TEM picture (a), three colours chemical cartography (b) and its representation per elemental cartography (Zn: c, O: d, Al: e) corresponding to 3 mol% Al-doped ZnO obtained under argon at 700 °C.

highest concentrations of aluminium are detected in the smallest grains. The presence of various grain sizes corresponding to various aluminium concentrations confirms that aluminium ions are segregated on the grains surfaces and the segregated aluminium ions act like a sintering-delay agent. The segregation of the Al^{3+} ions at the surface is induced by the easier relaxation of the first coordination spheres on grains surface than in bulk. Indeed, in grain bulk, the cations are fixed in tetrahedral coordination whereas the aluminium cations have got a strong preference for octahedral coordination. Moreover, one should notice that the surface energy (energy excess in comparison to the bulk) indicates lower stability of the surface local environments due to the reduction of their coordination number. Hence the introduction of an additive defect on surfaces (here Al^{3+} is located on zinc position) induces only a slight energy disequilibrium highlighting the competition between surface and bulk. To sum up, low temperature annealing allows the introduction of a higher Al concentration in doped ZnO powder than high temperature conditions; however, the aluminium cations are not well distributed, a segregation of the doping ions occurring near grain surface.

The last investigation concerns the impact of the Al^{3+} doping on the optical absorption properties obtained in the near-Infrared region. ZnO pure compound, and 1 and 3 mol% Al-doped ZnO obtained at 700 °C under argon (optimal conditions) were analysed by diffuse reflectance spectroscopy (Fig. 9). As previously discussed, the pure ZnO compounds exhibit non-negligible near-Infrared absorption due to its large specific surface with n-type intrinsic defects. Moreover, the introduction of 1 mol% of Al^{3+} cations leads to a significant increase of the Infrared absorption in regard of the undoped compound. The optical properties of the 1 and 3 mol% of Al^{3+} compounds are very close. The two samples exhibit a large Infrared absorption, which can be estimated to 78% (calculated by integration) between 800 and 2500 nm and 25% for the visible range absorption between 400 and 800 nm. These properties are very satisfying in regard of the requirements of thermal insulating films used in smart windows technology. Currently, the metallic films coated on windows to reject the solar heat (Infrared part of solar spectra) are not or very slightly selective between the transmission of the visible and the Infrared wavelength range. The similitude of the spectra of the 1 and 3 mol% Al-doped ZnO compounds indicates a similar free-carriers

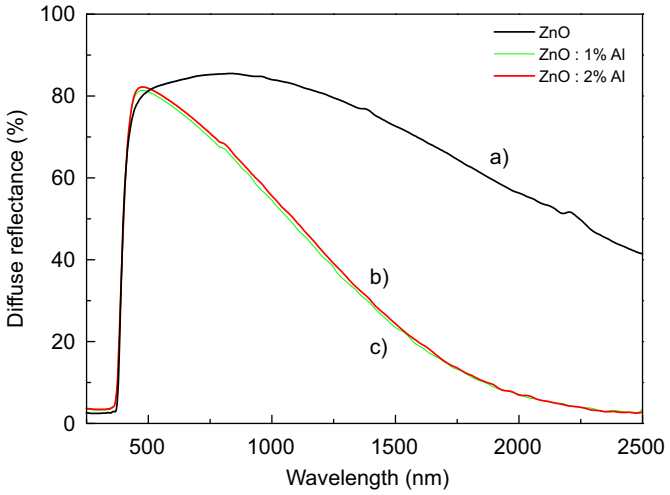

Fig. 9. Diffuse reflectance spectra of ZnO compounds obtained after thermal treatment at 700 °C under argon: (a) pure ZnO, (b) ZnO:Al(1%) and (c) ZnO–Al(3%).

concentration in the two doped samples. Hence, the high concentration of Al^{3+} ions introduced in zincite, thanks to the low temperature treatment used, is not plenty efficient. This could be due to the Al^{3+} segregation previously detected or because the optimal n-type carrier concentration was already reached for an Al doping concentration about 1 mol%. It can be also considered that, over a critical doping rate, the decrease of the charge mobility compensates the benefit of the doping concentration increase.

The near-Infrared absorption properties obtained for the Al-doped samples synthesised under argon are largely optimised besides the absorption of pure ZnO obtained under argon or Al-doped ZnO obtained under air atmosphere in our previous study [22]. Hence, in order to get the maximal Infrared absorption properties, it was shown here that one has to combine a "reductive" synthesis atmosphere, a low temperature route allowing the synthesis of highly divided powder and an aliovalent doping. Nevertheless, a critical doping rate over which the Infrared

absorption remains constant is quickly reached, showing a "saturation" of the system.

4. Conclusion

The pure ZnO oxides prepared in this study via a Pechini process exhibit Infrared absorption properties that depend on the atmosphere of synthesis and the grain size. In order to get the most important free-carrier concentration, low temperature and low pO_2 atmosphere have to be employed. Indeed, the combination of these synthesis parameters leads to highly divided powder within a high concentration of n-type defects mainly located on the grain surfaces.

The Al-doped ZnO oxides prepared under argon exhibit solubility limit largely over the ones previously reported for oxide prepared under air [22]. The solubility limit increases drastically while the grain size decreases when low temperature synthesis is performed. However, the solubility limit does not correspond only to the doping ions concentration that is homogeneously inserted in the material bulk. Actually, higher Al^{3+} ions rate can be introduced in divided powder samples with Al^{3+} segregation at the grain surface. However, the optical properties of the doped samples are to be correlated to the concentration inserted in the material bulk. Indeed, the concentration of "active" Al^{3+} cations on optical properties remains relatively low (under 1 mol%), far below the solubility limit.

Whatever, very satisfying optical properties in regard of the requirements of thermal insulating oxides are reached for the Al-doped ZnO powders prepared at low temperature under argon. The Al-doping of ZnO oxide with a synthesis route combining low pO_2 atmosphere and low annealing temperature leads to two positive effects: (i) creation of high free-carriers' concentration, which are mainly located on the grain surfaces; (ii) a large Al^{3+} concentration is also mainly located on grain surfaces. Thus, the combination of intrinsic and extrinsic defects at the surface, as well as into the bulk, contributes to enhance near-Infrared absorption properties.

In order to obtain optimal near-Infrared absorption properties for ZnO-based material, the key point is to combine the use of "low temperature synthesis", "reductive atmosphere" and "n-type aliovalent doping", substitution concentration over 1 mol% bringing no additional benefit.

References

[1] D.C. Altamirano-Juarez, G. Torres-Delgado, S. Jimenez-Sandoval, O. Jimenez-Sandoval, R. Castanedo-Perez, Solar Energy Materials and Solar Cells 83 (2004) 35.
[2] K.Y. Cheong, N. Muti, S.R. Ramanan, Thin Solid Films 440 (2002) 142.
[3] Roy G. Gordon, MRS Bulletin 25 (2000) 52.
[4] H. Mizoguchi, P.M. Woodward, Chemistry of Materials 16 (2004) 5233.
[5] Z. Ben Ayadi, L. El Mir, K. Djessas, S. Alaya, Nanotechnology 18 (2007) 445702.
[6] H. Gomez, A. Maldonado, R. Castanedo-Perez, G. Torres-Delgado, M. de la, L. Olivera, Materials Characterization 58 (2007) 708.
[7] M. Sugiyama, A. Murayama, T. Imao, K. Saiki, H. Nakanishi, S.F. Chichibu, Physica Status Solidi A 203 (2006) 2882.
[8] S. Major, A. Banerjee, K.L. Chopra, Thin Solid Films 122 (*1*) (1984) 31.
[9] W.W. Wenas, A. Yamada, K. Takahashi, M. Yoshino, M. Konagai, Journal of Applied Physics 70 (1991) 7119.
[10] T. Tsubota, M. Ohtaki, K. Eguchi, H. Arai., Journal of Materials Chemistry 7 (*1*) (1997) 85.
[11] K. Shirouzu, T. Ohkusa, M. Hotta, N. Enomoto, J. Hojo, Journal of the Ceramic Society of Japan 115 (1340) (2007) 254.
[12] T. Strachowski, E. Grzanka, W. Lojkowski, A. Presz, M. Godlewski, S. Yatsunenko, H. Matysiak, R.R. Piticescu, C.J. Monty, Journal of Applied Physics 102 (2007) 073513/1.
[13] D. Nie, T. Xue, Y. Zhang, X. Li, Science in China, Series B : Chemistry 51 (2008) 823.
[14] V.J. Norman, Australian Journal of Chemistry 22 (1969) 325.
[15] N. Roberts, R.-P. Wang, A.W. Sleight, W. Warren Jr., Physical Review B: Condensed Matter and Materials Physics 57 (1998) 5734.
[16] M.H. Yoon, S.H. Lee, H.L. Park, H.K. Kim, M.S. Jang, Journal of Materials Science Letters 21 (2002) 1703.
[17] K.H. Kim, S.H. Shim, K.B. Shim, K. Niihara, J. Hojo, Journal of the American Ceramic Society 88 (3) (2005) 628.
[18] K.F. Cai, E. Muller, C. Drasar, A. Mrotzek, Materials Science & Engineering B: Solid-State Materials for Advanced Technology B104 (2003) 45.
[19] G. Westin, M. Wijk, A. Pohl, Journal of Sol–Gel Science and Technology 31 (2004) 283.
[20] W. Shao, R. Ma, B. Liu, Journal of University of Science and Technology Beijing 13 (2006) 346.
[21] C. Kittel, E. Kolb, N. Bardon, Physique de l'état solide. Paris, 7th Edition, 1998.
[22] J.M. Ziman, Principles of Theory of Solids, 2nd Edition, Cambridge University Press, 1972.
[23] V. Srikant, D.R. Clarke, Journal of Applied Physics 83 (1998) 5447.
[24] H. Serier, M. Gaudon, M. Ménétrier, Solid State Sciences 11 (*7*) (2009) 1192.
[25] T. Izuma, K. Izumi, N. Kuroiwa, A. Senjuh, A. Fujimoto, M. Adachi, T. Yamamoto, Journal of Alloys and Compounds 480 (2009) 123.
[26] E. Burunkaya, N. Kariz, Ö. Kesmez, H.E. Camurlu, M. Asiltürk, E. Apaç, Journal of Sol–Gel Science Technology 55 (2010) 171.
[27] N. Pechini, US Patent No. 3,330,697, 1967.
[28] P.A. Lessing, American Ceramic Society Bulletin 68 (1989) 1002.
[29] H.M. Rietveld, Acta Crystallographica 22 (1967) 151.
[30] H.M. Rietveld, Journal of Applied Crystallography 2 (1969) 65.
[31] G.A. Parks, Chemical Reviews (Washington D.C.) 65 (1965) 177.
[32] F. Xu, P. Zhang, A. Navrotsky, Z. Yuan, T. Ren, M. Halasa, B. Su, Chemistry of Materials 19 (2007) 5680.
[33] L. Zhang, H. Cheng, R. Zong, Y. Zhu, Journal of Physical Chemistry C 113 (2009) 2368.